Radiation Oncology

Dosimetric evaluation of bone marrow sparing in proton radiotherapy for cervical cancer guided by MR functional imaging

Xiaohang Qin[1,2], Guanzhong Gong[2], Lizhen Wang[2], Ya Su[2] and Yong Yin[2*]

Abstract

Background: To segment the pelvic active bone marrow (PABM) using magnetic resonance (MR) functional imaging and investigate the feasibility and dosimetric characteristics of cervical cancer proton radiotherapy for active bone marrow (ABM) sparing.

Methods: We collected CT and MR simulation images of 33 patients with cervical cancer retrospectively. The PBM was contoured on the MRI FatFrac images; the PBM was divided into high-active bone marrow (ABM-$_{high}$) and low-active bone marrow based on the fat content of the PBM. Four radiotherapy plans were created for each patient, which included intensity-modulated photon therapy (IMRT), bone marrow sparing IMRT (IMRT-BMS), intensity-modulated proton therapy (IMPT), and bone marrow sparing IMPT (IMPT-BMS). The dosimetric differences among the four plans were compared.

Results: The ABM-$_{high}$ volume in the enrolled patients accounted for 45.2% of the total ABM volume. The target coverage was similar among the four radiotherapy plans. IMRT-BMS, IMPT, and IMPT-BMS reduced the D_{mean} of ABM-$_{high}$ by 16.6%, 14.2%, and 44.5%, respectively, compared to the D_{mean} of IMRT ($p < 0.05$). IMPT-BMS had the best protective effect on the bone marrow. Compared to IMRT, the volume of ABM-$_{high}$ receiving an irradiation dose of 5–40 Gy decreased by 10.2%, 36.8%, 58.8%, 67.4%, 64.9%, and 44.5%, respectively ($p < 0.001$).

Conclusions: The MR functional imaging technique helped in the grading and segmentation of PABM. MR functional image-guided proton radiotherapy for cervical cancer can achieve optimal BMS.

Keywords: Pelvic active bone marrow, Bone marrow sparing, Proton therapy, MR functional imaging, Cervical cancer

Background

Concurrent chemoradiotherapy can improve the clinical efficacy of cervical cancer treatment, but hematological toxicity (HT) can considerably decrease the survival time and quality of life of patients [1, 2]. Compared to radiotherapy alone, concurrent chemoradiotherapy affects the systemic immune response, resulting in a decrease

in compensatory responses in the bone marrow (BM) outside the pelvis and an increase in the incidence of HT [3–7]. The unavoidable dose of radiation to the pelvic active bone marrow (PABM) in cervical cancer radiotherapy is an important cause of HT. Low-dose irradiation of 10–20 Gy to PBM is the primary cause of HT [8–10]. In our previous study, we found a significant positive correlation between fat content changes in the 5–10 Gy irradiated PBM region and the nadir of lymphocytes and neutrophils during chemoradiotherapy [11]. A meta-analysis showed that bone marrow sparing (BMS) techniques could effectively reduce the bone marrow dose

*Correspondence: yinyongsd@126.com

[2] Department of Radiation Physics, Shandong Cancer Hospital and Institute, Shandong First Medical University and Shandong Academy of Medical Sciences, Jinan, China

Full list of author information is available at the end of the article

Qin *et al. Radiation Oncology* (2022) 17:207

Page 2 of 12

and the incidence of grade 2 or 3 HT by approximately 70% [12].

BM is divided into hematopoietic active bone marrow (ABM) and inactive BM, each accounting for approximately 50%. Approximately half of the ABM is distributed in the pelvic region. A dose of radiation to the ABM during radiotherapy is a major factor in the occurrence of acute HT. Various quantitative and qualitative imaging techniques help to accurately identify active fractions in the BM [13]. The accurate localization and sparing of ABM can reduce HT and improve tolerance to chemotherapy and survival rates [14, 15]. Magnetic resonance (MR) FatFrac imaging can be used to quantitatively analyze the fat content of the BM and can reflect the fat content changes in PBM during cervical cancer radiotherapy [11]. MR functional imaging provides a feasible method for ABM segmentation.

A photon-based BMS plan can effectively reduce the exposed volume of BM. The proton Bragg peak can further concentrate the dose to the target relative to the photon plan. Only a few fields are needed to meet the dose coverage of the target. Proton therapy has great potential for BMS due to its physical dose deposition properties that can effectively protect normal tissues adjacent to the target [16, 17]. Therefore, we used MR functional imaging to segment the PABM. We also analyzed the dosimetric differences between photon and proton BMS radiotherapy plans for cervical cancer. In this study, we determined the feasibility and dosimetric characteristics of MR functional imaging-guided BMS proton radiotherapy for cervical cancer.

Materials and methods

In total, 33 patients with cervical cancer who received concurrent chemoradiotherapy in Shandong Cancer Hospital from 2019 to 2020 were recruited. All patients received 45–50 Gy/25 fractions of pelvic intensity-modulated photon therapy (IMRT) combined with concurrent cisplatin chemotherapy. Each patient underwent CT and multi-sequence MR simulation scans. CT scans were performed using a Philips 16-slice Brilliance bigbore computed tomography scanner (Philips Medical Systems, Amsterdam, Netherlands) with a 3-mm slice gap thickness and 3-mm slice. The patients were immobilized in the supine position with thermoplastic molds or in the prone position with an abdominal pelvic fixator. Magnetic resonance imaging (MRI) was performed using a 3.0T superconducting MR scanner (Discovery 750w, GE Healthcare, USA) with the same position and fixed device as those used for the CT scans. All patients underwent T1WI, T2fs, and IDEAL IQ sequence scans with 3 mm slice thickness. The IDEAL IQ sequence scans were reconstructed to obtain the fat fraction (FatFrac IDEAL IQ) images.
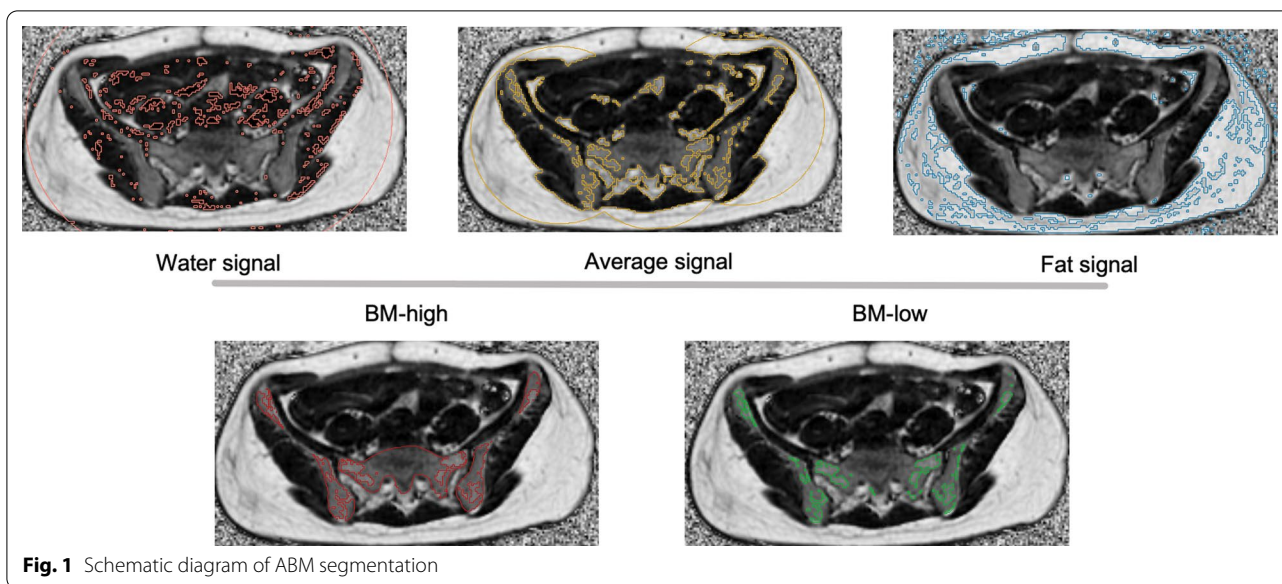
Target and BM contouring

The targets and organ at risk (OAR) were contoured on CT and MR fusion registration images. The gross tumor volume (GTV) of the uterus, cervix, parametrium, upper third of the vagina, and locoregional lymph nodes, which included common, internal and external iliac, obturator, and presacral lymph nodes, were all included in the clinical target volume (CTV). Then, 5 mm margins were added to the CTV while creating the planning target volume (PTV). OARs included the BM, bladder, rectum, spinal cord, left femoral head, and right femoral head.

The CT and MR simulation images were transmitted into MIM 7.1.7 (MIM Software Inc., Cleveland, OH, USA). Total ABM was contoured on the FatFrac images from the L4 vertebral body to the ischial tuberosities, including the sacrum, L4-5, and pelvis [18]. The signal values of urine in the bladder (defined as the water signal) and subcutaneous fat (defined as the fat signal) of each patient were measured separately on the FatFrac images. The average of the two signal values was defined as the segmentation threshold between high-active and low-active BM.

The threshold tool in MIM was used to contour high-active and low-active BM. The BM region with a signal value between the water signal and the segmentation threshold was defined as the high-active BM (ABM-$_{\text{high}}$), and that with a signal value between the segmentation threshold and the fat signal was defined as the low-active BM (ABM-$_{\text{low}}$) (Fig. 1). Segmented BM and ABM-$_{\text{high}}$ regions were superimposed (rigid registered) onto the CT simulation images. Finally, the CT images with BM and ABM-$_{\text{high}}$ structures were imported into the RayStation planning system.

Treatment planning

Treatment plans were created in RayStation Research v10.1B (RaySearch Laboratories, Stockholm, Sweden). Four types of treatment plans were created using standardized objectives: IMRT, bone marrow sparing IMRT (IMRT-BMS), intensity modulated proton therapy (IMPT), and bone marrow sparing IMPT (IMPT-BMS). The prescription dose was 45 Gy$_{\text{RBE}}$ in 25 fractions, with a single fraction dose of 1.8 Gy$_{\text{RBE}}$. A generic relative biological effectiveness (RBE) value of the proton dose was set to 1.1, and the photon dose RBE value was set to 1.0. The dose constraints for OARs were as follows [19]: bladder V_{30} (the percentage of the bladder volume irradiated with more than 30 Gy) $< 35\%$; femur head-L/R $V_{35} < 5\%$; rectum $V_{40} < 35\%$ and $V_{30} < 80\%$; the ABM $V_{10} < 80\%$, $V_{20} < 60\%$, $V_{30} < 45\%$, and $V_{40} < 30\%$.

Qin *et al. Radiation Oncology* (2022) 17:207

Page 3 of 12

Fig. 1 Schematic diagram of ABM segmentation

For the IMRT and IMRT-BMS treatment plans, nine coplanar fields were generated. All photon treatment plans were calculated using the Monte Carlo dose calculation algorithm and the DMLC technique based on the TureBeam linear accelerator (Varian Medical Systems, Palo Alto, CA, USA) with a 6-MV photon beam. As the primary objective, we aimed to reduce the percentage volume of ABM-$_{high}$ receiving 5–40 Gy as much as feasible when the target and other OARs were met the objectives.

For the IMPT and IMPT-BMS treatment plans, two posterior oblique beams (gantry angles of 150° and 210°)

and two semi-lateral beams (gantry angles of 85° and 275°) were used for the patients in the supine position (Fig. 2A). Two anterior oblique beams (gantry angles of 30° and 330°) and two semi-lateral beams (gantry angles of 85° and 275°) were used for the patients in the prone position (Fig. 2B). The pelvic target received a dose coverage from all four beams. Robust optimization was performed for the proton treatment plans, with a 3% range and a 0.3 cm set-up uncertainty in all orthogonal directions [20]. The Monte Carlo dose calculation algorithm with 1% uncertainty was used to calculate clinical dose distributions. The proton treatment plans were generated

Fig. 2 Schematic diagram of fields distribution for proton plans

Qin *et al. Radiation Oncology*   (2022) 17:207

Page 4 of 12
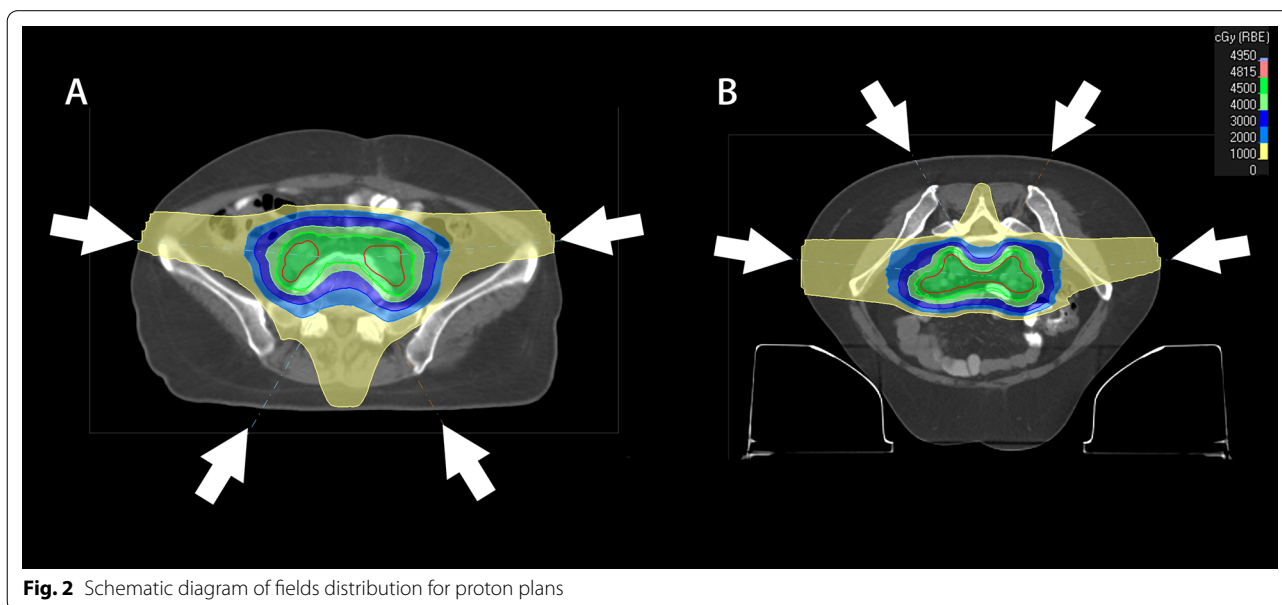
using a machine based on ProBeam with energy layer spacing of 1 cm and spot spacing of 0.75 cm.

For IMPT and IMPT-BMS, there were nine set-up errors and three range errors creating 27 individually "perturbed doses". For each target and OAR dose-volume objective evaluated, the static scenario (no error) and worst scenario were extracted from all the "perturbed doses", respectively.

Dosimetric evaluation and statistical analysis

CTV was used as the evaluation target volume for robustness optimization because PTV was used to account for delivery uncertainties that might change the intended CTV dose. For CTV, the dose of 2% and 98% volume ($D_{2\%}$, $D_{98\%}$) and the mean dose (D_{mean}) were analyzed. For OARs, the V_X (volume percent irradiated with xGy) and the D_{mean} were analyzed. To compare the results, the coverage of each treatment plan was normalized to the same level of 95% volume of the PTV received 100% prescription dose.

For evaluating the robustness of CTV coverage in each scenario, the median value of $D_{98\%}$, $D_{2\%}$, and D_{mean} in this scenario was compared to the prescription dose (45 Gy) by conducting one-sample Wilcoxon signed-rank tests. For evaluating the robustness of OAR and ABM in each scenario, the median values of various dose-volume metrics in this scenario were compared to the IMRT values by conducting paired Wilcoxon signed-rank tests. One-sample Wilcoxon signed-rank tests were conducted to analyze the dose volume parameters of the CTV and OARs for different body position.

Friedman's statistical test was conducted to determine whether there were any differences among the four treatment plans. Because the results of all Friedman's tests were significant, the differences among dose parameters were assessed using paired Wilcoxon signed-rank tests. All analyses were performed using IBM SPSS Version 25 (IBM SPSS Inc, Chicago, IL), and all differences were considered to be statistically significant at $p < 0.05$.

Results

BM location

The mean volume of BM in all patients was 299.37 cm^3 (191.32–417.54 cm^3). The average volume of ABM-$_{high}$ was 135.44 cm^3 (19.09–267.78 cm^3), accounting for 45.2% of the total ABM volume.

Robustness evaluation and body position evaluation

In all perturbed scenarios, the worst values for CTV $D_{98\%}$, $D_{2\%}$, and D_{mean} were similar to the prescribed dose. All the IMPT and IMPT-BMS worst scenario values for OAR were significantly better than or not different from IMRT values. The worst scenario values of ABM and ABM-$_{high}$

V_5-V_{40} and D_{mean} were all significantly lower than IMRT values. The data are shown in Additional file 1: Tables S1, S2, and S3.

The dose differences in different body positions are shown in Additional file 1: Tables S4, S5, and S6. In this study, there were 15 patients in the supine position and 18 patients in the prone position. The median volume of CTV was 521.26 mL and 585.88 mL, respectively. The target coverage between different body positions was similar. Compared to that in the supine position, the left and right femoral head and rectum V_{30} of the patients in the prone position increased slightly, and the doses of other OARs were similar. In IMPT, the V_{20}, V_{30} and D_{mean} of ABM and ABM-$_{high}$ in the prone position were higher than those in the supine position.

Dosimetric comparison between different treatment plans
IMRT versus IMPT

The CTV $D_{98\%}$ of the IMRT and IMPT treatment plans were similar. For IMPT, the CTV $D_{2\%}$ and D_{mean} were 0.6% and 0.4% higher than those for IMRT, respectively (Table 1). Compared to IMRT, IMPT decreased the D_{mean} of the bladder, the left, and right femoral heads, and the rectum by 17.1%, 2.6%, 2.6%, and 4.2%, respectively; the V40 of the bladder and the V_{30} of the rectum decreased by 3.2% and 8.6%, respectively ($p < 0.001$) (Table 2). The median reductions of the BM by IMPT were 0.8% for V_5, 8.6% for V_{10}, 25.3% for V_{20}, 15.5% for V_{30}, 9.6% for V_{40}, and 12.1% for D_{mean} (all $p < 0.05$) compared to the reduction by IMRT. ABM-$_{high}$ also decreased simultaneously by 0.6%, 8.2%, 23.5%, 15.8%, 6%, and 14.2% ($p < 0.05$) (Table 3).

IMRT versus IMRT-BMS

Compared to the IMRT treatment plans, the IMRT-BMS treatment plans had a similar CTV of $D_{98\%}$ ($p > 0.05$), and the IMRT-BMS plans had a slightly higher $D_{2\%}$ and D_{mean} (Table 1), which were approximately 1.1% and 0.7%, respectively ($p < 0.05$). The dose-volume parameters of all OARs in the two plans were similar ($p > 0.05$) (Table 2). The BM V_{10}, V_{20}, V_{30}, and D_{mean} decreased by 10.7%, 26.2%, 20.9%, and 14.8%, respectively; the ABM-$_{high}$ V_{10}, V_{20}, V_{30}, V_{40}, and D_{mean} decreased simultaneously by 10.2%, 26.3%, 24.1%, 13.6% and 16.6% ($p < 0.001$) (Table 3).

IMPT versus IMPT-BMS

Compared to that in the IMPT treatment plans, the CTV $D_{2\%}$ and D_{mean} in IMPT-BMS increased by 1.1% and 0.7%, respectively ($p < 0.05$) (Table 1). The V_{30} of the rectum and femoral heads decreased by 5.5% and 1.9%, respectively, in the IMPT-BMS and the V_{40} of the bladder decreased by 11.5% compared to that in the IMPT

Table 1 Dosimetric parameters of CTV for four types of plans

	OAR doses				Dose differences rate (*p* value)					
	IMRT	IMRT-BMS	IMPT	IMPT-BMS	IMRT versus IMPT	IMRT versus IMPT-BMS	IMPT versus IMPT-BMS	IMRT-BMS versus IMPT-BMS	IMRT-BMS versus IMPT	IMRT versus IMPT-BMS
CTV D$_{98\%}$										
Median	45.1	45	45.1	45.1	0%	− 0.2%	0%	0.2%	0.2%	0%
(min−max)	(44.8−45.3)	(44.8−45.3)	(44.8−45.4)	(45−45.3)	0.437	**0.001**	0.28	**< 0.001**	**0.048**	**< 0.001**
CTV D$_{2\%}$										
Median	46.3	46.6	46.8	47.3	1.1%	0.6%	1.1%	1.5%	0.4%	2.2%
(min−max)	(45.7−47.2)	(46−47.8)	(45.7−47)	(46.9−47.5)	**0.001**	**< 0.001**	**< 0.001**	**< 0.001**	0.064	**< 0.001**
CTV D$_{mean}$										
Median	45.6	45.8	45.9	46.2	0.7%	0.4%	0.7%	0.9%	0.2%	1.3%
(min−max)	(45.3−45.9)	(45.5−46.4)	(45.6−46)	(46−46.4)	**< 0.001**	**< 0.001**	**< 0.001**	**< 0.001**	0.064	**< 0.001**

Bold fonts indicate statistical significance (*p* < 0.05)

Qin *et al. Radiation Oncology* (2022) 17:207

Page 6 of 12

Table 2 Dosimetric parameters of OAR for four types of plans

Parameter	OAR doses				Dose differences rate (*p* value)					
	IMRT	IMRT-BMS	IMPT	IMPT-BMS	IMRT versus IMPT	IMRT versus IMRT-BMS	IMPT versus IMPT-BMS	IMRT-BMS versus IMPT-BMS	IMRT-BMS versus IMPT	IMRT versus IMPT-BMS
Bladder										
V_{40}										
Median	25.1	27.8	24.3	21.5	−3.2%	10.8%	−11.5%	−22.7%	−12.6%	−14.3%
(min–max)	(10.4–37.5)	(14.5–40.2)	(10.9–36)	(10.3–36.6)	**<0.001**	0.24	**0.001**	**<0.001**	**<0.001**	**<0.001**
D_{mean}										
Median	34.6	34.4	28.7	28.9	−17.1%	−0.6%	0.7%	−16.0%	−16.6%	−16.5%
(min–max)	(28.7–37.7)	(28.8–38.2)	(20.8–34.5)	(20.5–34.6)	**<0.001**	0.879	0.106	**<0.001**	**<0.001**	**<0.001**
Femur head—L										
V_{30}										
Median	9.3	6.2	5.2	5.1	−44.1%	−33.3%	−1.9%	−17.7%	−16.1%	−45.2%
(min–max)	(0–14.6)	(1.3–15.4)	(0.4–17.9)	(0.1–12.9)	0.503	0.126	**0.016**	**0.003**	0.469	**0.001**
D_{mean}										
Median	19.5	19.6	19	18.8	−2.6%	0.5%	−1.1%	−4.1%	−3.1%	−3.6%
(min–max)	(15.7–19.8)	(17.6–19.9)	(13.2–19.3)	(13.1–19.4)	**<0.001**	0.081	0.427	**<0.001**	**<0.001**	**<0.001**
Femur head—R										
V_{30}										
Median	8.8	5.7	5.2	5.1	−40.9%	−35.2%	−1.9%	−10.5%	−8.8%	−42.0%
(min–max)	(0–14.6)	(1.3–17)	(0.1–20.1)	(0.1–12.5)	0.136	0.079	**0.028**	**0.004**	0.9	**<0.001**
D_{mean}										
Median	19.6	19.5	19.1	19	−2.6%	−0.5%	−0.5%	−2.6%	−2.1%	−3.1%
(min–max)	(17.2–19.8)	(16.1–19.8)	(11–19.3)	(10.9–19.4)	**<0.001**	0.611	0.865	**<0.001**	**<0.001**	**<0.001**
Rectum										
V_{30}										
Median	71.8	82	65.6	62	−8.6%	14.2%	−5.5%	−24.4%	−20.0%	−13.6%
(min–max)	(36.5–96.9)	(37.4–97.8)	(23.3–70.2)	(22.8–70.5)	**<0.001**	0.299	**0.001**	**<0.001**	**<0.001**	**<0.001**
V_{40}										
Median	33.8	35.5	34.4	32.8	1.8%	5.0%	−4.7%	−7.6%	−3.1%	−3.0%
(min–max)	(6.9–37.1)	(8.1–40.4)	(11.3–37.1)	(9.6–37.8)	0.823	0.248	0.211	**<0.001**	**0.001**	0.761
D_{mean}										
Median	35.6	36.7	34.1	33.9	−4.2%	3.1%	−0.6%	−7.6%	−7.1%	−4.8%
(min–max)	(28.3–38.4)	(28.6–38.9)	(23–36.1)	(23.1–35.5)	**<0.001**	0.053	**0.03**	**<0.001**	**<0.001**	**<0.001**

Bold fonts indicate statistical significance ($p < 0.05$)

Qin *et al. Radiation Oncology*   (2022) 17:207

Page 7 of 12

Table 3 Dosimetric parameters of ABM and ABM$_{high}$ for four types of plans

Parameter	OAR doses				Dose differences rate (*p* value)					
	IMRT	IMRT-BMS	IMPT	IMPT-BMS	IMRT versus IMPT	IMRT versus IMRT-BMS	IMPT versus IMPT-BMS	IMRT-BMS versus IMPT-BMS	IMRT-BMS versus IMPT	IMRT versus IMPT-BMS
ABM										
V_5										
Median	100	100	99.2	91.3	− 0.8%	0%	− 8.0%	− 8.7%	− 0.8%	− 8.7%
(min–max)	(94.4–100)	(94.1–100)	(90.9–100)	(85.4–98.9)	**<0.001**	0.893	**<0.001**	**<0.001**	**<0.001**	**<0.001**
V_{10}										
Median	99.9	89.2	91.3	67.2	− 8.6%	− 10.7%	− 26.4%	− 24.7%	2.4%	− 32.7%
(min–max)	(90.4–100)	(76.7–95.6)	(75.5–95.7)	(56.7–78.3)	**<0.001**	**<0.001**	**<0.001**	**<0.001**	0.514	**<0.001**
V_{20}										
Median	91.7	67.7	68.5	39.8	− 25.3%	− 26.2%	− 41.9%	− 41.2%	1.2%	− 56.6%
(min–max)	(75.9–95.6)	(58.6–77.3)	(38.3–80)	(31–50.4)	**<0.001**	**<0.001**	**<0.001**	**<0.001**	0.922	**<0.001**
V_{30}										
Median	64.6	51.1	54.6	23.4	− 15.5%	− 20.9%	− 57.1%	− 54.2%	6.8%	− 63.8%
(min–max)	(44–76.5)	(39.3–56.6)	(25.7–89.6)	(16.1–35)	**<0.001**	**<0.001**	**<0.001**	**<0.001**	0.025	**<0.001**
V_{40}										
Median	24.9	24	27.3	10.9	9.6%	− 3.6%	− 60.1%	− 54.6%	13.8%	− 56.2%
(min–max)	(13.1–38.1)	(15.5–35.5)	(10.5–38.9)	(6.4–23.1)	**0.017**	0.256	**<0.001**	**<0.001**	**<0.001**	**<0.001**
D_{mean}										
Median	33.1	28.2	29.1	19.4	− 12.1%	− 14.8%	− 33.3%	− 31.2%	3.2%	− 41.4%
(min–max)	(29–39.7)	(26.4–32.7)	(23.6–35.87)	(17.7–28.5)	**<0.001**	**<0.001**	**<0.001**	**<0.001**	**0.081**	**<0.001**
ABM$_{high}$										
V_5										
Median	100	100	99.4	89.8	− 0.6%	0%	− 9.7%	− 10.2%	− 0.6%	− 10.2%
(min–max)	(92.9–100)	(92.7–100)	(87.8–100)	(80.5–98)	**<0.001**	0.249	**<0.001**	**<0.001**	**<0.001**	**<0.001**
V_{10}										
Median	99.9	89.7	91.7	63.1	− 8.2%	− 10.2%	− 31.2%	− 29.7%	2.2%	− 36.8%
(min–max)	(87–100)	(82.4–98.6)	(78–99.2)	(58.7–70.9)	**<0.001**	**<0.001**	**<0.001**	**<0.001**	**0.001**	**<0.001**
V_{20}										
Median	91.8	67.7	70.2	37.8	− 23.5%	− 26.3%	− 46.2%	− 44.2%	3.7%	− 58.8%
(min–max)	(80–97.9)	(36.3–86.4)	(47.1–93.2)	(31.2–45.1)	**<0.001**	**<0.001**	**<0.001**	**<0.001**	0.118	**<0.001**
V_{30}										
Median	66.5	50.5	56	21.7	− 15.8%	− 24.1%	− 61.3%	− 57.0%	10.9%	− 67.4%
(min–max)	(50.8–90.9)	(42.9–74.1)	(35.9–89.8)	(18.9–27.9)	**<0.001**	**<0.001**	**<0.001**	**<0.001**	**0.006**	**<0.001**
V_{40}										

Qin *et al. Radiation Oncology*   *(2022) 17:207*

Page 8 of 12

Table 3 (continued)

Parameter	OAR doses			Dose differences rate (*p* value)					
	IMRT	IMRT-BMS	IMPT	IMPT-BMS	IMRT versus IMPT	IMRT versus IMRT-BMS	IMPT versus IMPT-BMS	IMRT-BMS versus IMPT-BMS	IMRT-BMS versus IMPT	IMRT versus IMPT-BMS
Median	30.2	26.1	32	10.6	6.0%	− 13.6%	− 66.9%	− 59.4%	22.6%	− 64.9%
(min–max)	(17.7–61.1)	(17.9–40)	(16.6–55.3)	(6.6–14.7)	**0.037**	**0.04**	**0.001**	**0.001**	**0.001**	**0.001**
D_{mean}										
Median	33.7	28.1	28.9	18.7	− 14.2%	− 16.6%	− 35.3%	− 33.5%	2.8%	− 44.5%
(min–max)	(29–39.7)	(26.4–32.7)	(23.6–35.87)	(17.7–28.5)	**< 0.001**	**< 0.001**	**< 0.001**	**< 0.001**	0.081	**< 0.001**

Bold fonts indicate statistical significance (*p* < 0.05)

Qin *et al. Radiation Oncology*   (2022) 17:207

Page 9 of 12

plan ($p < 0.05$) (Table 2). IMPT-BMS decreased the BM V_{10}-V_{40} and the D_{mean}, and the reduction range of each index was 15.5%–47.1%. The ABM-$_{high}$ showed a similar trend, where the V_{10}-V_{40} and the D_{mean} decreased by 9.7%, 31.2%, 46.2%, 61.3%, 66.9%, and 35.3%, respectively ($p < 0.001$) (Table 3).

IMRT-BMS versus IMPT-BMS

Compared to that in the IMRT-BMS treatment plans, the CTV $D_{98\%}$, $D_{2\%}$, and D_{mean} increased by 0.2%, 1.5%, and 0.9% in the IMPT-BMS treatment plans, respectively (Table 1). The dose-volume parameters of all OARs in the IMPT-BMS plan were lower than those in the IMRT-BMS plan, with the greatest reductions in bladder-V_{40} and rectum-V_{30} by 22.7% and 24.4%, respectively (Table 2). IMPT-BMS performed better than IMRT-BMS. The V_5-V_{40} and D_{mean} of BM and ABM-$_{high}$ were reduced by the IMPT-BMS plans compared to their values in the IMRT-BMS plans. The reductions were as follows: 8.7% and 10.2% for V_5, 24.7% and 29.7% for V_{10}, 41.2% and 44.2% for V_{20}, 54.2% and 57% for V_{30}, 54.6% and 59.4% for V_{40}, and 31.2% and 33.5% for D_{mean} ($p < 0.001$) (Table 3).

IMRT-BMS versus IMPT

Compared to the IMRT-BMS plans, the IMPT plans had a similar CTV $D_{2\%}$ and D_{mean}, and the CTV $D_{98\%}$ increased in IMPT with differences within the 0.2% range (Table 1). IMPT plans significantly decreased the V_{40} of the bladder and V_{30} of the rectum by 12.6% and 20%, respectively ($p < 0.001$). ABM-$_{high}$ V_{10}-V_{40} and D_{mean} increased in IMPT plans compared to that in IMRT-BMS, and the V_{40} had a larger increase of 22.6% ($p < 0.001$). The BM showed a similar trend of change (Table 3).

IMRT versus IMPT-BMS

Compared to the IMRT plans, the IMPT-BMS plans had similar CTV $D_{98\%}$ and a slightly higher CTV $D_{2\%}$ and D_{mean} (2.2% and 1.3%, respectively) (Table 1). All dose-volume parameters of OARs increased significantly using the IMPT-BMS plans (Table 2). The volume reductions are presented as follows: 45.2% and 42% for V_{30} of the left and right femoral head, 14.3% for V_{40} of the bladder, and the D_{mean} of bladder decreased from 34.6 Gy to 28.9 Gy (by 16.5%), 13.6% for V_{30} of the rectum, and the D_{mean} of the bladder decreased from 35.6 Gy to 33.9 Gy (by 4.8%) ($p < 0.001$). The V_5-V_{40} and D_{mean} of BM decreased by 8.7%, 32.7%, 56.6%, 63.8%, 56.2%, and 41.4%, respectively. Similarly, the V_5-V_{40} and D_{mean} of ABM-$_{high}$ decreased by 10.2%, 36.8%, 58.8%, 67.4%, 64.9%, and 44.5% ($p < 0.001$) (Table 3).
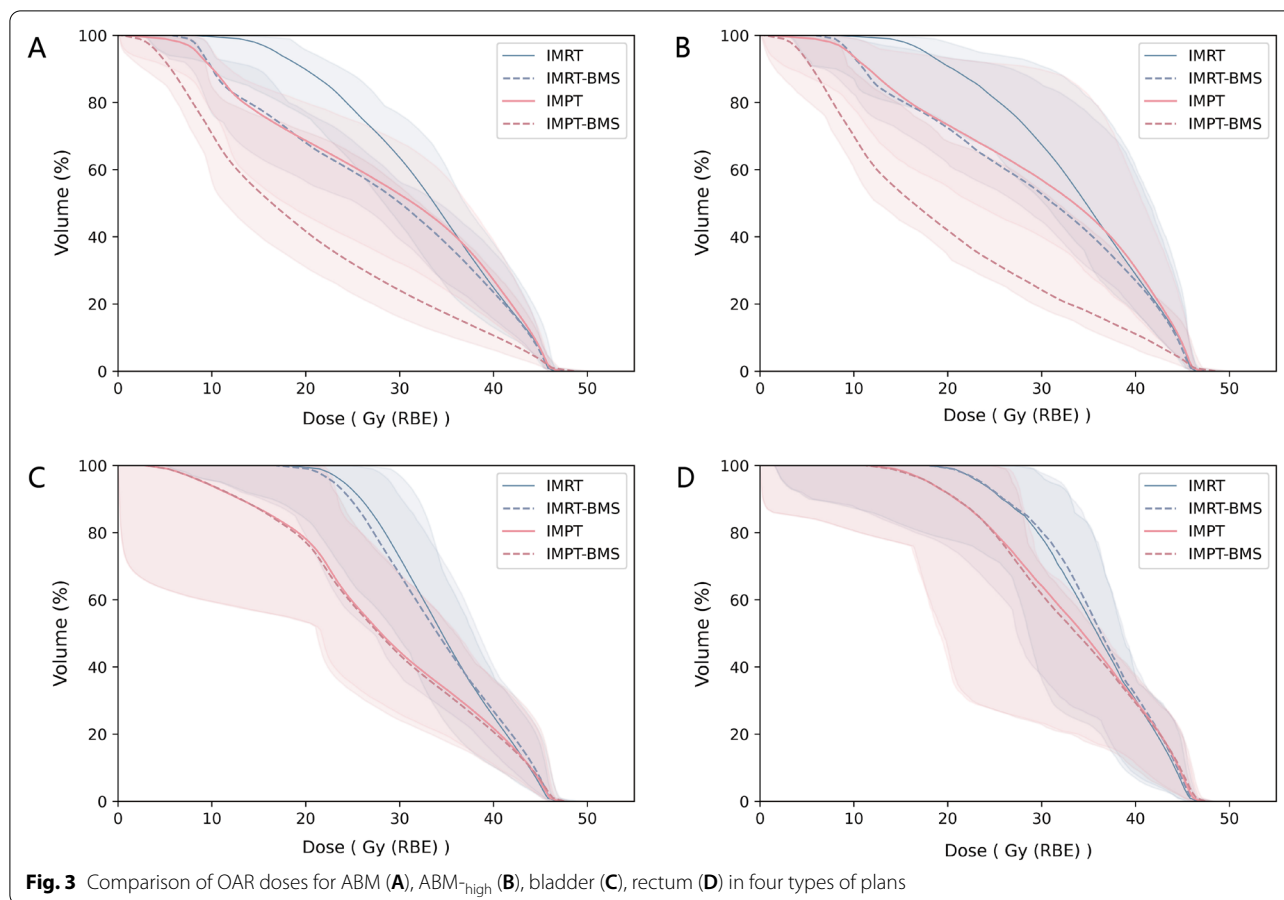
Although the CTV parameters differed significantly among the four plans, the absolute difference was low, and all four types of plans had the ideal target volume coverage. IMPT-BMS showed the highest BM sparing without compromising target volume dose coverage, which significantly decreased the V_{10}-V_{40} and D_{mean} of ABM-$_{high}$. Additionally, IMRT-BMS reduced the dose for ABM-$_{high}$ than IMRT but increased the dose in the bladder and rectum (Fig. 3).

Discussion

In this study, we investigated the role of functional MR imaging combined with proton therapy on BMS in cervical cancer radiotherapy. Our results confirmed the feasibility of using functional MR imaging to segment high-active BM and the dosimetric advantage of proton therapy for BMS, especially PABM. Huang et al. [21] reported that 69.5% of the patients with cervical cancer who received concurrent chemoradiotherapy experienced G2+HT. For every 1 Gy increase in the D_{mean} of PBM, the neutrophils and white blood cells of the patient decreased by 9.6/μL and 7.8/μL each week, respectively [22]. Radiation-induced lymphopenia can be associated with lower survival [23, 24]. Kumar et al. [10] reported that G4 HT was associated with PBM $V_{20} > 45\%$. In many studies, PBM V_{20} was significantly associated with HT, and V_{40} was an important predictor of G2+HT [12, 14]. The HT produced during concurrent chemoradiotherapy can last for at least three months after treatment is completed [25, 26].

The BM dose-volume parameter is the main index for predicting HT. However, many studies have used different prediction indices and dose-volume parameters, and no ideal radiation dose limitation for BM has been suggested yet. This can be associated with different definitions of the BM region used in various studies. Accurate identification and delineation of PABM are important. Most studies use CT bone window images to contour BM. However, no unified standard is available for BM delineation. CT images cannot distinguish BM activity, and there is a large error in delineation. PET/CT can segment actively proliferating BM regions based on tissue metabolism. However, the cost of PET/CT examination is high, the clinical popularity is poor, and the risk of radiation exists. MR functional imaging not only accurately delineates the BM region but also distinguishes and segments the ABM through the water-fat separation technique [27–29]. In another study, we reported that IDEAL IQ FatFrac imaging could be used to measure PBM fat content changes during concurrent chemoradiotherapy. The fat content of PBM increased with the increase in radiotherapy dose, especially in the PBM region close to the target region receiving high-dose irradiation (the fat fraction increased from 48.5% to 74.2%), and the change was significantly related to the HT [11]. Liang et al. [18] used the FatFrac image to contour the PBM for the

Qin *et al. Radiation Oncology*   (2022) 17:207

Page 10 of 12

Fig. 3 Comparison of OAR doses for ABM (**A**), ABM-$_{high}$ (**B**), bladder (**C**), rectum (**D**) in four types of plans

IMRT-BMS plan design, which can reduce the incidence of G3 + HT from 47 to 30%. In this study, we established a method for ABM segmentation. The average value of the water and fat signal values in the FatFrac IDEAL IQ image was selected as the segmentation threshold of the ABM, and the threshold contour tool was used to manually segment the ABM. The results showed that highly active bone marrow accounted for about 45% of the total ABM volume and was dispersed, which was consistent with the results of studies by Liang and other researchers [18].

Many previous studies have been based on photon radiotherapy planning for BMS. However, some limitations are present due to the radiation dose constraints of photon beams on BM. The physical properties of protons can reduce proximal dose deposition compared with photons. The finite range and sharp distal fall-off characteristics of protons allow radiation dose to be delivered to a specific depth using the spread-out Bragg peak. The distant normal tissue receives a negligible radiation dose [16, 30]. More conformal dose distributions can be achieved due to the ability of IMPT to control the

beamlet energies and intensities. The irradiation dose of BM can be further reduced based on IMRT-BMS. Dinges et al. [20] used FLT-PET/CT to identify PABM in patients with cervical cancer. Compared to IMRT, the V_{10}-V_{40} reduction of ABM in the IMPT plan ranged from 32 to 60%. This was consistent with the results of this study that IMPT-BMS can reduce ABM-$_{high}$ V_{10}-V_{40} by 29.7%–59.4% compared to IMRT-BMS. Lin et al. [31] demonstrated the dosimetric advantages and clinical feasibility of pencil beam scanning, and the PBM volume was significantly reduced by 24% and 17% in 10–20 Gy low-dose irradiation. Meier et al. [32] compared IMPT and VMAT cervical cancer BMS plan and found that the D_{mean} of BM decreased from 30.76 Gy to 17.42 Gy. This was similar to the results of this study, where we found that IMPT-BMS reduced the D_{mean} of ABM-$_{high}$ from 33.7 Gy to 18.7 Gy (by 44.5%).

By comparing four types of radiotherapy plans in this study, we found that the use of proton therapy increased the protection of PABM in the low-dose region. IMRT-BMS plans set dose constraints on ABM-$_{high}$ based on IMRT plans, reducing ABM-$_{high}$ V_{10}-V_{40} and D_{mean}.

Qin *et al. Radiation Oncology*   (2022) 17:207

Page 11 of 12

However, the ability of IMRT-BMS to modulate the dose is still limited. The dose-volume parameters of the bladder and rectum tend to increase while reducing the dose of ABM-$_{high}$. IMPT-BMS uses the exquisite physical dose deposition characteristics of the proton beam, which can further reduce the ABM-high V_{10}-V_{40} and D_{mean} based on IMRT-BMS. The D_{mean} of ABM-$_{high}$ was as low as 18.7 Gy to achieve the best bone marrow sparing effect. IMPT-BMS can also allow significant sparing of normal tissues such as the bladder and rectum.

Since protons have a larger penumbra, normal tissues near the target may receive a higher radiation dose [16]. Xu et al. [33] reported that compared to IMRT, proton therapy performed poorly in decreasing the irradiated volume of PBM in the high-dose region (33.9–42.9 Gy), and the PBM V_{40} increased by 14.6%. In this study, IMPT ABM-$_{high}$ V_{30} and V_{40} were 10.9% and 22.6% higher than IMRT-BMS, respectively. This was associated with the region of ABM-$_{high}$ irradiated > 30 Gy adjacent to the target volume without dose constraints to the bone marrow. IMRT-BMS was a better choice than IMPT. After setting ABM-$_{high}$ dose constraints in IMPT, ABM-$_{high}$ V_{30} and V_{40} were reduced by 61.3% and 66.9%, respectively, and the D_{mean} decreased from 28.9 Gy to 18.7 Gy compared to that of IMRT-BMS.

We evaluated the feasibility of PABM delineation based on FatFrac images and bone marrow sparing with proton therapy from a dosimetric perspective only. This should be further applied to actual treatment to evaluate the effect of differences in dose reduction between different radiotherapy techniques on the risk of HT. Reliable BM radiation dose limits should be set to guide individualized radiation therapy for bone marrow sparing.

Our findings confirmed that IMPT-BMS uses its dosimetric advantage to achieve optimal BMS in radiotherapy for cervical cancer without compromising target dose volume coverage. We proposed a threshold delineation of PABM by FatFrac images, which provided a new method for PABM segmentation. MR functional imaging guidance can reduce the irradiation dose volume of PABM, and MR functional imaging combined with proton therapy can achieve optimal bone marrow sparing in radiotherapy for cervical cancer.

Abbreviations

PABM: Pelvic active bone marrow; MR: Magnetic resonance; ABM: Active bone marrow; ABM-$_{high}$: High-active bone marrow; IMRT: Intensity modulated photon therapy; IMRT-BMS: Bone marrow sparing IMRT; IMPT: Intensity modulated proton therapy; IMPT-BMS: Bone marrow sparing IMPT; HT: Hematological toxicity; BM: Bone marrow; BMS: Bone marrow sparing; FatFrac IDEAL IQ: Fat fraction; OAR: Organ at risk; GTV: Gross tumor volume; CTV: Clinical target volume; PTV: Planning target volume; ABM-$_{low}$: Low-active BM; RBE: Relative biological effectiveness.

Supplementary Information

Additional file 1. Supplementary data. **Table S1** Statistics for CTV in IMPT and IMRT-BMS in static and worst scenarios. **Table S2** Statistics for OAR in IMPT and IMRT-BMS in static and worst scenarios. **Table S3** Statistics for PABM in IMPT and IMRT-BMS in static and worst scenarios. **Table S4** Dose differences in different body positions of CTV. **Table S5** Dose differences in different body positions of OAR. **Table S6** Dose differences in different body positions of ABM and ABM-$_{high}$.

Availability of data and materials
All data obtained during the current study are available from the corresponding author on reasonable request.

Declarations

Ethics approval and consent to participate
This study was reviewed and approved by the Institutional Review Board of Shandong Cancer Hospital. Patients were required to provide written informed consent to participate in this research.

Consent for publication
Not applicable.

Competing interests
The authors declare that they have no competing interests.

Author details
[1]Department of Graduate, Shandong First Medical University, Shandong Academy of Medical Sciences, Jinan, China. [2]Department of Radiation Physics, Shandong Cancer Hospital and Institute, Shandong First Medical University and Shandong Academy of Medical Sciences, Jinan, China.

References

1. Mell LK, Xu R, Yashar CM, et al. Phase 1 trial of concurrent gemcitabine and cisplatin with image guided intensity modulated radiation therapy for locoregionally advanced cervical carcinoma. Int J Radiat Oncol Biol Phys. 2020;107(5):964–73.
2. Corbeau A, Kuipers SC, de Boer SM, et al. Correlations between bone marrow radiation dose and hematologic toxicity in locally advanced cervical cancer patients receiving chemoradiation with cisplatin: a systematic review. Radiother Oncol. 2021;164:128–37.
3. Vitzthum LK, Heide ES, Park H, et al. Comparison of hematologic toxicity and bone marrow compensatory response in head and neck vs. cervical cancer patients undergoing chemoradiotherapy. Front Oncol. 2020;10:1179.

Qin *et al. Radiation Oncology*   (2022) 17:207

Page 12 of 12

4. Robinson M, Muirhead R, Jacobs C, et al. Response of FDG avid pelvic bone marrow to concurrent chemoradiation for anal cancer. Radiother Oncol. 2020;143:19–23.

5. Williamson CW, Sirák I, Xu R, et al. Positron emission tomography-guided bone marrow-sparing radiation therapy for locoregionally advanced cervix cancer: final results from the INTERTECC phase II/III Trial. Int J Radiat Oncol Biol Phys. 2022;112(1):169–78.

6. Yu DY, Bai YL, Feng Y, et al. Which bone marrow sparing strategy and radiotherapy technology is most beneficial in bone marrow-sparing intensity modulated radiation therapy for patients with cervical cancer? Front Oncol. 2020;10:554241.

7. van Meir H, Nout RA, Welters MJ, et al. Impact of (chemo)radiotherapy on immune cell composition and function in cervical cancer patients. Oncoimmunology. 2016;6(2):e1267095.

8. Rose BS, Aydogan B, Liang Y, et al. Normal tissue complication probability modeling of acute hematologic toxicity in cervical cancer patients treated with chemoradiotherapy. Int J Radiat Oncol Biol Phys. 2011;79(3):800–7.

9. Albuquerque K, Giangreco D, Morrison C, et al. Radiation-related predictors of hematologic toxicity after concurrent chemoradiation for cervical cancer and implications for bone marrow-sparing pelvic IMRT. Int J Radiat Oncol Biol Phys. 2011;79(4):1043–7.

10. Kumar T, Schernberg A, Busato F, et al. Correlation between pelvic bone marrow radiation dose and acute hematological toxicity in cervical cancer patients treated with concurrent chemoradiation. Cancer Manag Res. 2019;11:6285–97.

11. Wang C, Qin X, Gong G, Wang L, Su Y, Yin Y. Correlation between changes of pelvic bone marrow fat content and hematological toxicity in concurrent chemoradiotherapy for cervical cancer. Radiat Oncol. 2022;17(1):70.

12. Zhou P, Zhang Y, Luo S, et al. Pelvic bone marrow sparing radiotherapy for cervical cancer: A systematic review and meta-analysis. Radiother Oncol. 2021;165:103–18.

13. Mell LK. Trials and tribulations of bone marrow sparing radiotherapy for cervical cancer. Re: Zhou et al. Radiother Oncol. 2021;165:103–118. Radiother Oncol. 2022;167:78–80.

14. Leake RL, Mills MK, Hanrahan CJ. Spinal marrow imaging: clues to disease. Radiol Clin North Am. 2019;57(2):359–75.

15. Franco P, Arcadipane F, Ragona R, et al. Hematologic toxicity in anal cancer patients during combined chemo-radiation: a radiation oncologist perspective. Expert Rev Anticancer Ther. 2017;17(4):335–45.

16. Mohan R. A review of proton therapy—Current status and future directions. Prec Radiat Oncol. 2022;1–13.

17. Gort EM, Beukema JC, Matysiak W, et al. Inter-fraction motion robustness and organ sparing potential of proton therapy for cervical cancer. Radiother Oncol. 2021;154:194–200.

18. Liang Y, Bydder M, Yashar CM, et al. Prospective study of functional bone marrow-sparing intensity modulated radiation therapy with concurrent chemotherapy for pelvic malignancies. Int J Radiat Oncol Biol Phys. 2013;85(2):406–14.

19. Pötter R, Tanderup K, Kirisits C, et al. The EMBRACE II study: The outcome and prospect of two decades of evolution within the GEC-ESTRO GYN working group and the EMBRACE studies. Clin Transl Radiat Oncol. 2018;9:48–60.

20. Dinges E, Felderman N, McGuire S, et al. Bone marrow sparing in intensity modulated proton therapy for cervical cancer: Efficacy and robustness under range and setup uncertainties. Radiother Oncol. 2015;115(3):373–8.

21. Huang J, Gu F, Ji T, et al. Pelvic bone marrow sparing intensity modulated radiotherapy reduces the incidence of the hematologic toxicity of patients with cervical cancer receiving concurrent chemoradiotherapy: a single-center prospective randomized controlled trial. Radiat Oncol. 2020;15(1):180.

22. Zhu H, Zakeri K, Vaida F, et al. Longitudinal study of acute haematologic toxicity in cervical cancer patients treated with chemoradiotherapy. J Med Imaging Radiat Oncol. 2015;59(3):386–94.

23. Wang Y, Deng W, Li N, et al. Combining immunotherapy and radiotherapy for cancer treatment: current challenges and future directions. Front Pharmacol. 2018;9:185.

24. Venkatesulu BP, Mallick S, Lin SH, et al. A systematic review of the influence of radiation-induced lymphopenia on survival outcomes in solid tumors. Crit Rev Oncol Hematol. 2018;123:42–51.

25. Elicin O, Callaway S, Prior JO, et al. [(18)F]FDG-PET standard uptake value as a metabolic predictor of bone marrow response to radiation: impact on acute and late hematological toxicity in cervical cancer patients treated with chemoradiation therapy. Int J Radiat Oncol Biol Phys. 2014;90(5):1099–107.

26. Sapienza LG, Salcedo MP, Ning MS, et al. Pelvic insufficiency fractures after external beam radiation therapy for gynecologic cancers: a meta-analysis and meta-regression of 3929 patients. Int J Radiat Oncol Biol Phys. 2020;106(3):475–84.

27. Ma Q, Cheng X, Hou X, et al. Bone marrow fat measured by a chemical shift-encoded sequence (IDEAL-IQ) in patients with and without metabolic syndrome. J Magn Reson Imaging. 2021;54(1):146–53.

28. Yang H, Cui X, Zheng X, et al. Preliminary quantitative analysis of vertebral microenvironment changes in type 2 diabetes mellitus using FOCUS IVIM-DWI and IDEAL-IQ sequences. Magn Reson Imaging. 2021;84:84–91.

29. Bolan PJ, Arentsen L, Sueblinvong T, et al. Water-fat MRI for assessing changes in bone marrow composition due to radiation and chemotherapy in gynecologic cancer patients. J Magn Reson Imaging. 2013;38(6):1578–84.

30. Taunk N. The role of proton therapy in gynecological radiation oncology. Int J Gynecol Cancer. 2022;32(3):414–20.

31. Lin LL, Kirk M, Scholey J, et al. Initial report of pencil beam scanning proton therapy for posthysterectomy patients with gynecologic cancer. Int J Radiat Oncol Biol Phys. 2016;95(1):181–9.

32. Meier T, Mascia A, Wolf E, et al. Dosimetric comparison of intensity-modulated proton therapy and volumetric-modulated arc therapy in anal cancer patients and the ability to spare bone marrow. Int J Part Ther. 2017;4(2):11–7.

33. Xu MJ, Maity A, Vogel J, et al. Proton therapy reduces normal tissue dose in extended-field pelvic radiation for endometrial cancer. Int J Part Ther. 2018;4(3):1–11.

Publisher's Note